Combust. Sci. Technol., 187: 1065–1078, 2015

ISSN: 0010-2202 print / 1563-521X online
DOI: 10.1080/00102202.2014.993033

Taylor & Francis
Taylor & Francis Group

THERMAL AND ELECTROLYTIC DECOMPOSITION AND IGNITION OF HAN–WATER SOLUTIONS

Prashant Khare,[1] Vigor Yang,[1] Hua Meng,[2] Grant A. Risha,[3] and Richard A. Yetter[3]

[1]*School of Aerospace Engineering, Georgia Institute of Technology, Atlanta, Georgia, USA*

[2]*School of Aeronautics and Astronautics, Zhejiang University, Hangzhou, Zhejiang Province, China*

[3]*Department of Mechanical and Nuclear Engineering, Pennsylvania State University, University Park, Pennsylvania, USA*

Thermal and electrolytic decomposition and ignition of water solutions of hydroxylammonium nitrate (HAN, $[NH_3OH]^+[NO_3]^-$) are investigated. Experiments are conducted to demonstrate the feasibility of electrolytic ignition for HAN-based ionic liquid propellants. As a consequence of electrolysis, the propellant decomposes to NH_2OH, HNO_3, HONO, HNO, N_2O, N_2, NO, NO_2, H_2O, $H_2(g)$, and $O_2(g)$. These species then initiate a series of gas phase reactions, governed by the H–O–N kinetics scheme, and lead to ignition. Electrochemical mechanisms are established and incorporated into an existing chemical kinetics scheme for thermal decomposition of HAN–water solutions. The analysis treats the liquid and gas phases separately, and matches their respective processes at the interfacial boundary to determine the overall decomposition and ignition characteristics. Results are benchmarked against experimental data for the species evolution in the condensed phase, as well as laser-induced ignition delay of 13 M HAN–water solution. The effects of electric current (0–2.5 A), propellant volume (0.1–0.3 cc), initial temperature (300–450 K), and HAN concentration (9–13 M) on the ignition behaviors are investigated systematically. The ignition delay decreases with increasing electric current as a power-law function: $\tau_{ign} = AI^{-n}$, where $A = 3.95$ and $n = 0.95$ for a 0.1 cc 13 M HAN–water solution at an initial condition of 300 K and 1 atm. The exponent n and coefficient A are decreasing functions of the initial temperature. For a given power, decreasing the initial volume of HAN–water solution increases the current density available for electrolysis, and expedites the ignition process. The work represents the first theoretical study of its kind on this topic.

Keywords: Electrolytic ignition; Green propellants; HAN; Ignition; Liquid monopropellants

INTRODUCTION

The quest for reduced hazards and environmentally benign properties has led to consideration of hydroxylammonium nitrate (HAN) and its derivatives as potential propellants

Received 18 August 2014; revised 27 October 2014; accepted 25 November 2014.

Address correspondence to Vigor Yang, School of Aerospace Engineering, Georgia Institute of Technology, 270 Ferst Drive, 313 Montgomery Knight Building, Atlanta, GA 30332-0150, USA. E-mail: vigor.yang@aerospace.gatech.edu

Color versions of one or more of the figures in the article can be found online at www.tandfonline.com/gcst.

for various propulsion applications, and as a replacement for commonly used hypergolic propellants such as hydrazine. HAN, with the chemical formula $[NH_3OH]^+[NO_3]^-$, exhibits strong ion–ion interactions, with $[NH_3OH]^+$ as the cation and $[NO_3]^-$ as the anion. The latter has a resonance structure, and two electrons are shared between three N–O bonds (Wei et al., 2006). HAN is a water soluble ionic solid and serves as the primary oxidizer when used in bi-propellant systems. HAN-based monopropellants usually employ alcohol as the fuel with HAN as the oxidizer in a single solution. As the concentration of HAN increases, the liquids become more electrolytic and prone to ignition with application of a low voltage. Table 1 presents a comparison of performance between HAN-based propellants and hydrazine (Gordon and McBride, 1994). In spite of its relatively lower specific impulse I_{sp}, HAN offers considerably higher density-I_{sp}, a feature of significance for volume-limited systems. For example, HAN-based AF-M315E has recently been considered as a potential candidate for microthrusters and micro-spacecrafts for attitude control (Hawkins et al., 2010).

Table 2 lists the physiochemical properties of HAN (Ashcraft et al., 2007; Courthéoux et al., 2006; Kuwahara et al., 1997; Mueller, 1999). HAN-based formulations are noncarcinogenic, nonflammable, and non-explosive at atmospheric pressure, and have a vapor head composed only of water (Jankovsky and Oleson, 1997). Hydrazine has a Lethal Dose50[1] (LD_{50}) value of 59 mice as compared to 325 rats (Anflo et al., 2002) for HAN-based propellants, clearly indicating the merits of HAN over hydrazine in terms of toxicity.

Table 1 Performance parameters of HAN-based monopropellants and hydrazine

Propellant	Vacuum I_{sp} @ 1 atm (s) (Gordon and McBride, 1994)	Density (kg/m^3) (Lee and Litzinger, 2001)	Density $I_{sp} \times 10^3$ (kg/m^3-s)
Hydrazine	227.35	1003.7	228.19
HAN (100%)	217.85	1830.0	398.67
13 M[a] HAN-water soln.	168.35	1537.0	258.75
10.7 M[a] HAN-water soln.	135.50	1449.0	196.34

[a]Molarity, M, is defined as the number of moles of the solute in 1 L of the solvent.

Table 2 Physiochemical properties of HAN

Freezing point (K) 75/25 HAN–water solution	243 (Mueller, 1999)
Melting point (K) (pure HAN)	321 (Courthéoux et al., 2006)
Density (kg/m^3) @ 298K	1830 (Kuwahara et al., 1997)
Enthalpy of formation (kcal/mol)	−79.68 (Ashcraft et al., 2007)
Toxicity (LD_{50} orally mg/kg)	325 rats (Anflo et al., 2002)

[1]LD_{50}, a standard measure for expressing and comparing the toxicity of chemicals, is defined as the dose that kills half (50%) of the animals, e.g., rats or mice, tested. Common units are milligram of chemical per kilogram of the test animal (mg/kg).

Table 3 Laser-induced ignition delay times in air and argon at 1 atm*

Propellant	In air	In argon
HAN (13 M)	3.0–4.5	2.5–5.0
TEAN	~1.0	2.5–3.5
XM46	1.0–2.7	2.7–4.0

*Laser heat flux of 400 W/cm^2 (unit: s) (Lee and Litzinger, 1999).

Since solid crystalline HAN is not capable of self-sustained burning at atmospheric pressure (Kondrikov et al., 2000), experimental studies have in the past been conducted on propellants based on water solutions of HAN such as XM46 [60.8 wt% HAN, 19.2 wt% triethanolammonium nitrate (TEAN), and 20 wt% H_2O] to characterize their ignition and combustion behavior (Beyer et al., 2000; Beyer & Reeves, 1997; Comer, 1977; Juvan and Beyer, 1999; Katsumi et al., 2012; Kim et al., 1997; Lee and Litzinger, 2001; Lee and Litzinger, 1999; McQuaid et al., 1998; McQuaid et al., 1998; Van Dijk & Priest, 1984; Vosen, 1989). Laser-induced ignition experiments were conducted on 5–30 cm^3 of XM46 by Beyer and Reeves (1997) at 1 atm pressure using a three-stage initiator. Increasing volumes of 0.1, 1.54, and 16.1 cm^3 were used in a multistage initiator such that each chamber vents tangentially into the next larger volume, thereby transferring the ignition kernel. It was concluded that ignition of a large volume of the liquid propellant is difficult to achieve in an open vessel, but modest pre-pressurization can readily lead to ignition of XM46 for chamber sizes of practical interest. Further studies on the ignition kinetics of XM46 were conducted, and global (one-step) reaction rates were obtained for a temperature range of 300–1200 K at pressures of 6.9 and 9.7 MPa (Beyer et al., 2000). Lee and Litzinger (1999) conducted laser assisted ignition experiments on XM46 and its ingredients, HAN and TEAN, over a pressure range of 0.1–1 atm and heat fluxes of 50–400 W/cm^2. Table 3 summarizes the results, where ignition was defined as the first appearance of visible light emission.

Electrolysis has recently been suggested as a viable means of ignition for applications in microscale thrusters (Risha et al., 2007), mainly due to the advantages of efficient thermal management, low ignition temperature, reduced power requirements, enhanced system durability and reliability, and reduced cost. The objectives of this paper are twofold: (1) to demonstrate the feasibility of using electrolysis for ignition of ionic liquid propellant XM46 and (2) to develop a numerical model for investigating the thermal and electrolytic ignition characteristics of HAN–water solutions.

The rest of the article is organized in three sections. The first section describes a proof-of-concept experiment. Then we present the electrochemical mechanisms and theoretical formulation. Since limited literature exists on detailed and quantitative liquid- and gas-phase reaction mechanisms of XM46, effort is focused on HAN–water solutions. The study helps to establish a solid basis for comprehensive understanding of the ignition process of ionic liquid propellants. Following that, we discuss laser (thermal)- and electrolytic-induced decomposition and ignition of HAN–water solutions. The present work represents the first theoretical study of its kind on this topic.

EXPERIMENT

Experiments are conducted to investigate the feasibility of electrolytic gasification and ignition of HAN-based XM46 propellant at room conditions. Figure 1 shows the

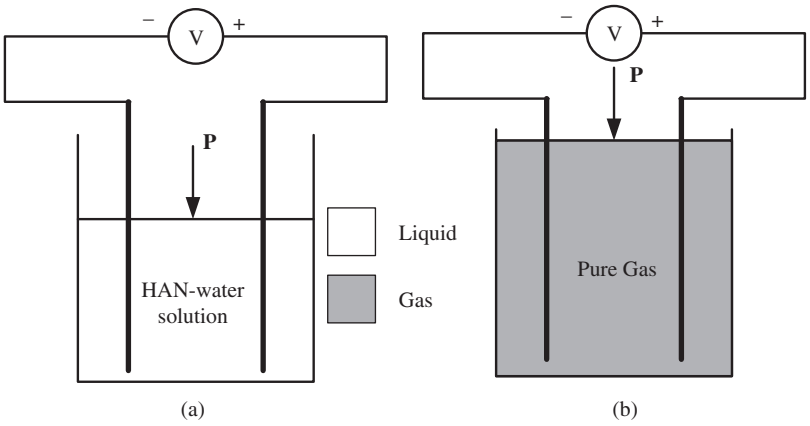

Figure 1 Experimental setup for electrolytic induced ignition of HAN–water solutions.

experimental setup. A titanium microfin electrode module is used, which consists of eight evenly spaced parallel fins with dimensions of 9 × 19 × 0.25 mm, and each separated by 1 mm. The electrode surface area ranged from 1050–4200 mm^2, and the input voltage from 7–26 V (Risha et al., 2007). The surface area is changed by controlling the submersion depth of electrodes in the liquid propellant. The experiment resembles a liquid strand burner, where the propellant, if ignited, bubbles and establishes a downward propagating, self-sustaining combustion wave. Potential difference is applied across the electrodes to initiate electrolysis of the liquid. Measurements are made of the temporal evolution of the electrode amperage, voltage, and liquid temperature. Voltage is removed as soon as the electric current reaches its peak value. The test is terminated by diluting the mixture with water.

Figure 2 shows the time history of events during the electrolytic gasification of 15 mL XM46 at 15 V. The bubbling process starts immediately after the voltage supply is switched on. At t = 0.07 s, violent gasification of XM46 is observed throughout the electrode surface. Peak reactivity, the point at which maximum electric current flows through the liquid propellant, is achieved at ∼0.75 s. After this, the power decreases due to increased resistivity through the liquid/gas mixture. The phenomenon is indicative of the maximum ionic transport through the liquid medium. The time delay to peak reactivity decreases

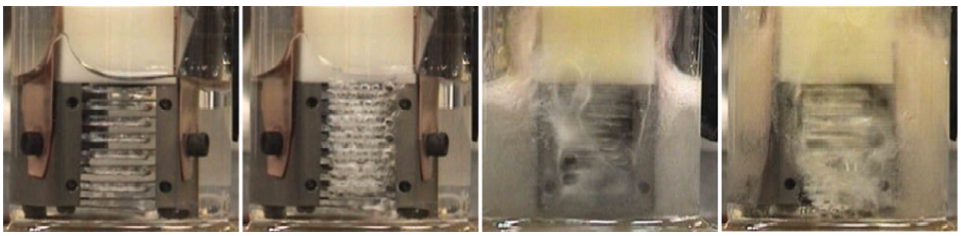

Figure 2 Gasification study of XM46 using electrolysis (Risha et al., 2007).

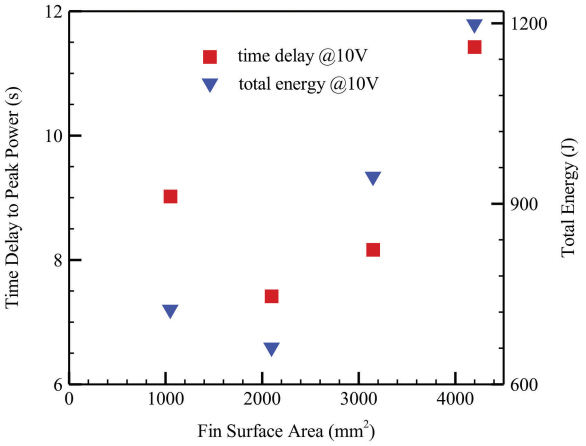

Figure 3 Time delay to peak power and total energy to achieve peak reactivity as a function of electrode surface area for electrolytic gasification of XM46 at voltage input of 10 V (Risha et al., 2007).

exponentially with increasing input voltage up to 12 V. The propellant temperature reached a steady state value of 115 °C, independent of input voltage, which is consistent with the data reported in Chang et al. (2001). Figure 3 shows the measurements of time delay to peak power and total energy as a function of electrode surface area for input voltages of 10–12 V. The time delay and total energy reaches a minimum at 2100 mm^2, making this the optimal submersion depth from an efficiency standpoint. Results also suggest that a higher input voltage promotes quicker gasification while consuming considerably less energy.

ELECTROCHEMICAL KINETICS AND THEORETICAL FORMULATION

Liquid water can be electrolyzed to produce protons and electrons on the anode as follows:

$$H_2O \rightarrow \frac{1}{2}O_2 + 2H^+ + 2e^- \tag{R1}$$

The proton produced during the electrolysis process promotes the following HAN decomposition reaction

$$(NH_3OH)^+(NO_3)^- + H^+ \rightarrow HNO_3 + (NH_3OH)^+ \tag{R2}$$

The overall electrochemical reaction on the anode side takes the form

$$2(NH_3OH)^+(NO_3)^- + H_2O \rightarrow \frac{1}{2}O_2 + 2HNO_3 + 2(NH_3OH)^+ + 2e^- \tag{R3}$$

Since $(NH_3OH)^+$ exists in high concentrations in the HAN–water solution, it migrates toward the cathode and is reduced by the electron, which arrives at the cathode through the external circuit. The electrochemical-reduction reaction on the cathode side is given by (R4):

$$2(NH_3OH)^+ + 2e^- \rightarrow 2NH_2OH + H_2 \quad \text{(R4)}$$

The combination of (R3) and (R4) yields the global reaction arising from electrolysis:

$$2(NH_3OH)^+(NO_3)^- + H_2O \rightarrow 2HNO_3 + 2NH_2OH + H_2 + \frac{1}{2}O_2 \quad \text{(R5)}$$

In addition to anodic and cathodic electrochemical reactions, thermal decomposition of HAN is considered to accurately model HAN decomposition by electrolysis. Table 4 summarizes these reactions, (R6)–(R16), along with their reaction rates and activation energies. A total of 10 initial decomposition steps, (R3), (R4), and (R6)–(R13), are included in the present analysis, involving 12 species: HAN, NH_2OH, HNO_3, HONO, HNO, N_2O, N_2, NO, NO_2, H_2O, H_2, and O_2. Among them, H_2 and O_2 appear only in the gaseous phase. HNO_3, N_2O, N_2, NO, NO_2, and H_2O may evaporate and exist in both the condensed and gaseous phases, as represented by reactions (R14)–(R16). The gaseous species produced by the condensed-phase reactions subsequently initiate a series of gas-phase reactions governed by the H-O-N kinetics scheme. The gas-phase mechanism consists of 32 species and 151 reactions, which are described in detail elsewhere (Khare, 2009; Thakre et al., 2014; Yang et al., 2005).

A constant-pressure, adiabatic, homogeneous reactor model is formulated to study the ignition characteristics of HAN–water solutions. The species conservation equation for the condensed phase is written as follows:

$$\frac{\partial(m_c Y_i)}{\partial t} = -\delta_i \frac{s_i I}{nF} MW_i + \dot{\omega}_i MW_i V_c - k_{l\rightarrow g,i} m_c Y_i \quad (1)$$

The source terms on the right-hand side arise from electrochemical reactions, (R3)–(R4); chemical reactions, (R6)–(R13); and evaporation processes, (R14)–(R16), respectively. The parameters, m_c and V_c, stand for the mass and volume of the condensed phase; Y_i and MW_i are the mass fraction and molecular weight of species i; and t, I, and F are the time, electric current, and the Faraday constant (96487 C/mol), respectively. The chemical production rate, $\dot{\omega}_i$, takes the form

Table 4 Reaction rates and activation energies (Lee and Litzinger, 2003)

Reaction	A[a]	E[b]	
$HAN + H_2O \rightarrow NH_2OH + HNO_3 + H_2O^{**}$	1.7 e10 ± 9.3 e2	15.1 ± 0.5	R6
$NH_2OH + HNO_3 \rightarrow HONO + NHO + H_2O^{**}$	3.7 e4 ± 8.9 e3	6.6 ± 0.7	R7
$NH_2OH + HONO \rightarrow N_2O + 2H_2O^{**}$	7.8 e4 ± 4.5 e3	3.3 ± 0.2	R8
$NH_2OH + HNO \rightarrow N_2 + 2H_2O^{**}$	1.5 e5 ± 2.4 e2	2.7 ± 0.1	R9
$3HONO \rightarrow 2NO + HNO_3 + H_2O^{***}$	1.5 e13 ±5.3 e2	9.1 ± 0.2	R10
$2HNO \rightarrow N_2O + H_2O^{**}$	7.5 e13 ± 58	17.1 ± 0.1	R11
$HNO + HNO_3 \rightarrow 2HONO^{**}$	7.5 e8 ± 0.3	16.6 ± 0.1	R12
$HONO + HNO_3 \rightarrow 2NO_2 + H_2O^{**}$	0.3 ± 1.8 e2	0.7 ± 0.1	R13
$(k_{l\rightarrow g})_{N_2O,N_2,NO,NO_2}$	2.7 e3 ± 5.9	2.4 ± 0.1	R14
$(k_{l\rightarrow g})_{H_2O}$	3.9 e5 ± 1.1 e2	9.9 ± 0.1	R15
$(k_{l\rightarrow g})_{HNO_3}$	3.6 e5 ± 2.0 e3	12.8 ± 0.6	R16

[a]Unit of A: * 1/s, ** (cm^3/mol) /s, *** (cm^3/mol)^2/s.
[b]Unit of E: (kcal/mol).

$$\dot{\omega}_i = \sum_{j=1}^{M} \nu_{ji} k_j \prod_{i=1}^{N} [\chi_i]^{\nu_{ji}} \tag{2}$$

where M stands for the number of chemical reactions, N is the number of species, and k_j is the rate coefficient of the jth reaction in the Arrhenius form. The electrochemical term in Eq. (1) is formulated in the following general form:

$$\sum_i s_i M_i = ne^- \tag{3}$$

The parameter M_i represents any chemical component in the electrochemical reaction, s_i is the stoichiometric number, and n is the number of electrons. The parameter δ_{i} is defined as

$$\delta_i = \begin{cases} 1 & \text{for } HAN, HNO_3, NH_2OH, H_2O \\ 0 & \text{for all other species} \end{cases} \tag{4}$$

The energy equation for the condensed phase can be written as follows:

$$\frac{dH_c}{dt} = -\sum_i \dot{m}_{l\to g,i}\, h_{fg,i} + VI + q \tag{5}$$

where H_c is the total enthalpy in the condensed phase and V is the applied voltage. The three terms on the right-hand side represent the contributions from vaporization, energy addition by the electrolysis process, and external heat sources, respectively. The species and energy conservation equations for the gas phase can be found elsewhere (Khare, 2009).

The physiochemical processes in the liquid and gas phases are treated separately. They are matched at the interfacial boundary by enforcing the continuities of mass and energy at each time step. The procedure eventually determines the overall decomposition and ignition characteristics of the mixture. Details of the numerical algorithm are given in Khare (2009). A comprehensive review of the techniques used for modeling energetic-material combustion and ignition can be found in Beckstead et al. (2007).

RESULTS AND DISCUSSION

The theoretical formulation and numerical analysis are first validated against the experimental data of Lee and Litzinger (2003) for the species evolution in the condensed phase during decomposition of 13 M HAN–water solution at an isothermal condition of 195 °C. The electrolytic and external heat-source terms in Eqs. (1) and (4) are switched off to model this process. Decomposition reactions, (R6)–(R16), are used for this analysis. The experimentally measured temperature is correlated using a sixth-order polynomial and used in the present analysis as a known variable, as shown in Figure 4a. Excellent agreement with experimental data (Lee and Litzinger, 2003) are obtained for the temporal evolution of HAN, HNO_3, H_2O, and NH_2OH (see Figure 4b). Decomposition begins with rapid disintegration of HAN into NH_2OH and HNO_3. Simultaneously, the mass fraction of H_2O decreases due to evaporation. HAN and H_2O are almost completely consumed by 0.5 s.

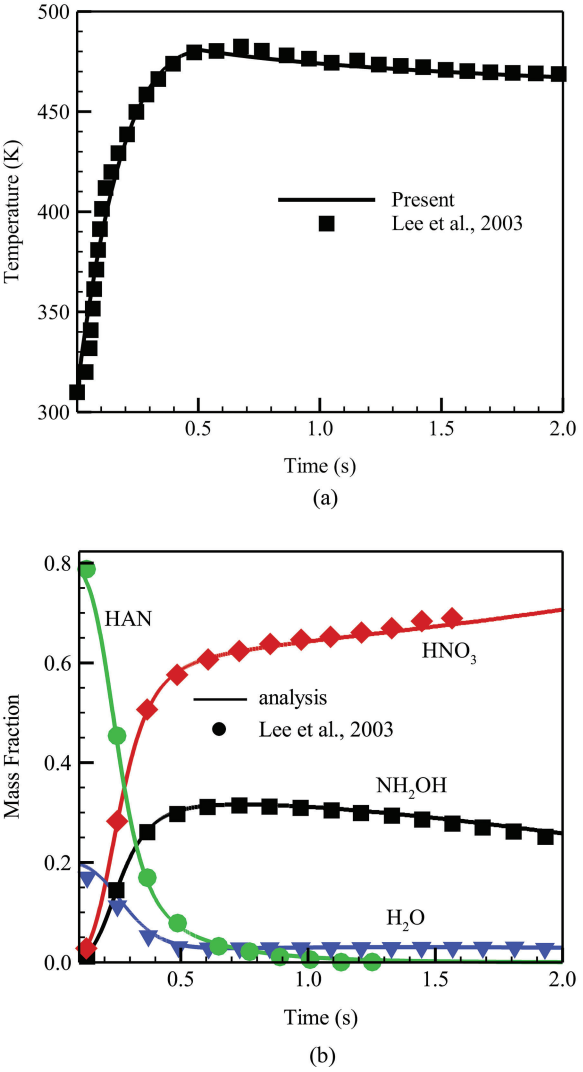

Figure 4 Temporal evolution of condensed phase temperature and species mass fractions for ignition of 13 M HAN solution at a set temperature of 195 °C.

The numerical structure of the gas-phase analysis is benchmarked against results obtained from the CHEMKIN code for propane/air ignition over a broad range of temperatures and pressures. The evolution of temperature and species closely matches reference data. Details of the numerical algorithm and flame structure can be found in Meng et al. (2009).

Laser-Induced Ignition

Laser-induced ignition of 0.3 cc 13 M HAN–water solution at an initial condition of 300 K and 1 atm is studied to provide a detailed description of the flame structure.

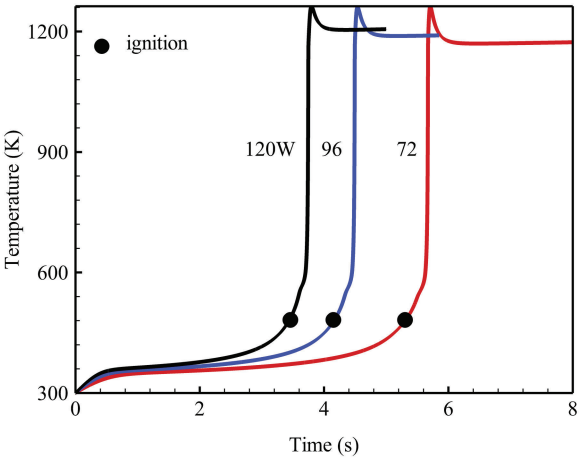

Figure 5 Temperature evolution: laser-induced ignition of 0.3 cc 13 M HAN–water solution. P = 1 atm, T = 300 K.

It also serves as a validation case to benchmark the numerical model and gas-phase chemistry against measured ignition delay (Lee and Litzinger, 1999). The laser energy flux of 400 W/cm^2 used in the experiment is translated to the total power input of 120 W into a test sample 0.3 cc solution with a height of 10 mm. Because the amount of energy absorbed by the HAN–water solution and the temporal behavior of the laser were not quantified in the experiment, the present numerical analysis is performed using a homogeneous heating term with power inputs in the range of 72–120 W. For this analysis, the electrolytic terms in the conservation equations are switched off, while the external heat source q is kept intact to simulate laser-assisted thermal ignition.

Figure 5 shows the temperature evolution with three different power inputs. Ignition is defined by thermal runaway in the current analysis. The point of inflection ($d^2T/dt^2|_{\tau_{ign}} = 0$ with $d^2T/dt^2|_{\tau_{ign}+\varepsilon}$ and $d^2T/dt^2|_{\tau_{ign}-\varepsilon}$ having opposite signs in the neighborhood of τ_{ign}) is used to quantitatively identify the ignition time delay. The temperature rapidly increases immediately following ignition and reaches its maximum value. Table 3 shows wide scatter in measured ignition delay of HAN, TEAN, and XM46. This may be attributed to the high sensitivity of such experiments to initial conditions (Lee and Litzinger, 1999). For a power input of 120 W (identical to the experiment condition), the calculated results show excellent agreement with measurements. The simulations for 72 W and 96 W represent conditions when only a portion of laser energy (ranging from 60 to 80%) is absorbed. Figure 6 shows the time histories of the temperature and species mass fractions at a power input of 120 W. The ignition delay corresponds to the rapid decay of HAN and $H_2O(l)$ and production of water vapor. This observation is supported by previous experiments (Kim et al., 1997; Lee and Litzinger, 1999). The mass fractions of major gaseous species NO, NO_2, and HNO_3 grow gradually and reach their peak values sharply at the point of ignition.

Electrolytic Ignition

Electrolytic ignition of HAN–water solutions is studied in terms of the effects of the initial temperature, electric current, volume, and HAN concentration. The pressure and

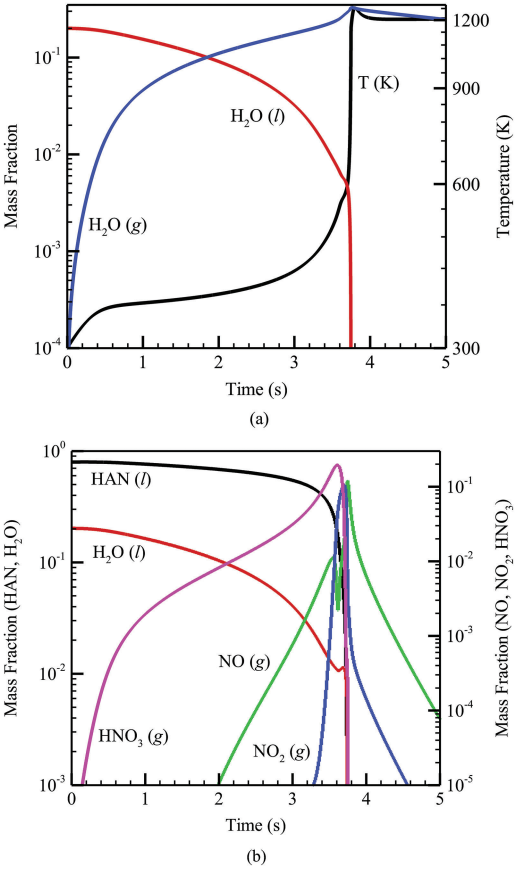

Figure 6 Evolution of temperature and species mass fractions during laser ignition of 0.3 cc 13 M HAN–water solution at a power input of 120 W.

applied voltage are fixed at 1 atm and 28 V, respectively, and the current varies in the range of 0–2.5 A. A 0.1 cc 13 M solution is considered at initial temperatures of 300–450 K. The electrolytic terms in the governing equations are switched on to simulate electrolysis and subsequent ignition.

The ignition delay decreases with increasing initial temperatures (see Figure 7). Figures 7–9 show that the ignition delay decreases with increasing electric current as a power-law function: $\tau_{ign} = AI^{-n}$, where $A = 3.95$ and $n = 0.95$ for an initial condition of 300 K and 1 atm. Increasing the current enhances electrolytic breakdown of the ionic propellant, thus increasing the reaction rate and expediting the ignition process. The exponent n and coefficient A are decreasing functions of the initial temperature. As compared to thermal ignition, for example, at 300 K and 1 atm, the reduction in the ignition delay is about 32% when 0.3 cc of 13 M HAN–water solution is ignited using electrolysis for a power input of 120 W. This illustrates the potential advantages of using electrolysis for ignition of liquid ionic propellants.

Since the electrolytic-induced HAN ignition is also intended for propulsion applications in small-scale devices, the effect of propellant volume on the ignition process is

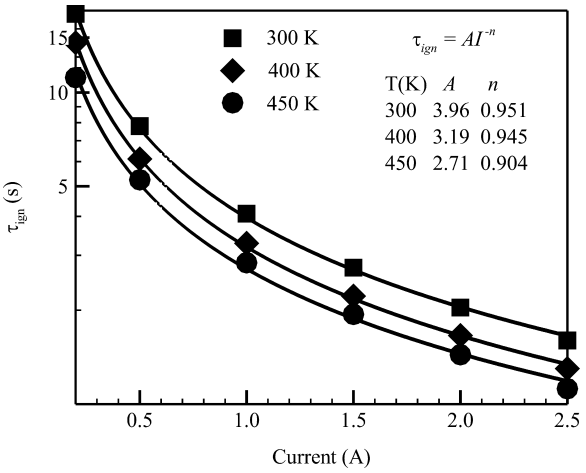

Figure 7 Effect of initial temperature on electrolytic ignition time delay of 0.1 cc 13 M HAN–water solution.

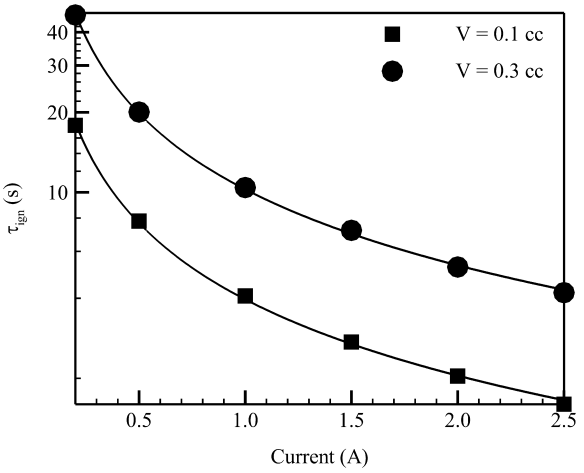

Figure 8 Effect of propellant volume on electrolytic ignition time delay of 13 M HAN–water solution at 300 K.

examined by considering a 13 M HAN–water solution at 300 K. Figure 8 shows that for a given input power, 0.1 cc solution ignites much faster than 0.3 cc. Decreasing the propellant volume increases the current density available for electrolysis, thereby facilitating the ignition process. The effect of increased current density is manifested via two mechanisms: enhanced breakdown of the ionic propellant by electrolysis and increased heating of the liquid due to the augmented heat source.

Figure 9 shows that for 0.1 cc of the propellant at an initial temperature of 300 K, ignition delay increases as the HAN concentration decreases from 13 M to 9 M. Vaporization of water is a precursor to ignition of HAN–water solutions (Kim et al., 1997; Lee and Litzinger, 1999). Low molarity translates to a higher water content and subsequently increases the ignition delay. In summary, high values of current, HAN concentration, and initial temperature, and low propellant volume are favorable conditions to achieve faster ignition.

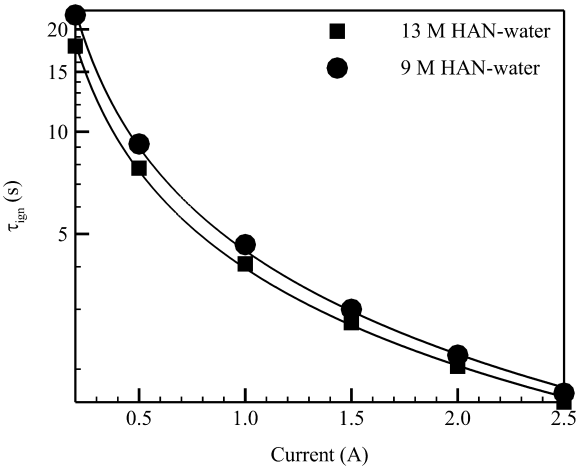

Figure 9 Effect of HAN concentration on electrolytic ignition time delay of 0.1 cc HAN–water solution at 300 K.

CONCLUSIONS

In this article, thermal and electrolytic decomposition and ignition of HAN-based propellants were studied theoretically and experimentally. Reactions governing the electrolysis of ionic liquids were established and combined with an existing chemical kinetics scheme (Lee and Litzinger, 2003) for thermal decomposition of HAN–water solutions. A theoretical model was developed based on the assumptions of a homogeneous, constant pressure reactor and employed in the analysis. Results indicate that electric current significantly reduces the ignition delay, and it varies as a power-law function: $\tau_{ign} = AI^{-n}$. For a given power, decreasing the initial propellant volume increases the current density available for electrolysis and expedites the ignition process. The electrolytically induced ignition of HAN-based ionic liquid propellants is especially appropriate for applications in small-scale propulsion devices.

ACKNOWLEDGMENT

The support and encouragement provided by Dr. Mitat Birkan, contract monitor, is gratefully acknowledged.

FUNDING

This work was sponsored in part by Air Force Office of Scientific Research, Grant Number FA9550-04-1-0291, and in part by the William R. T. Oakes endowment of the Georgia Institute of Technology.

REFERENCES

Anflo, K., Gronland, T.A., Bergman, G., Johansson, M., and Nedar, R. 2002. Towards green propulsion for spacecraft with ADN-based monopropellants. Presented at the 38th AIAA/ASME/SAE/ASEE Joint Propulsion Conference & Exhibit, Indianapolis, IN, July 7–10. AIAA-2002-3847, AIAA, Reston, VA.

Ashcraft, R.W., Raman, S., and Green, W.H. 2007. Ab initio aqueous thermochemistry: Application to the oxidation of hydroxylamine in nitric acid solution. *J. Phys. Chem. B*, **111**, 11968–11983.

Beckstead, M.W., Puduppakkam, K., Thakre, P., and Yang, V. 2007. Modeling of combustion and ignition of solid-propellant ingredients. *Prog. Energy Combust. Sci*., **33**, 497–551.

Beyer, R.A., Cohen, A., Von Wahlde, R., and Newberry, J.E. 2000. A study of the ignition kinetics of XM46. ARL-TR-2353, U.S. Army Research Laboratory, Aberdeen Proving Ground, MD.

Beyer, R.A., and Reeves, G.P. 1997. Laser ignition of liquid propellant XM46: Ignition of larger volumes. ARL-TR-1292, U.S. Army Research Laboratory, Aberdeen Proving Ground, MD.

Chang, Y., Boyer, E., and Kuo, K. 2001 Combustion behavior and flame structure of XM46 liquid propellant. *J. Propul. Power*, **17**, 800–808.

Comer, R.H. 1977. Ignition and combustion of liquid monopropellants at high pressures. *Proc. Combust. Inst*., **16**, 1211–1219.

Courthéoux, L., Amariei, D., Rossignol, S., and Kappenstein, C. 2006. Thermal and catalytic decomposition of HNF and HAN liquid ionic as propellants. Appl. Catal., B, **62**, 217–225.

Gordon, S., and McBride, B.J. 1994. Computer program for calculation of complex chemical equilibrium composition and applications.NASA RP-1311-P2.

Hawkins, T.W., Brand, A.J., McKay, M.B., and Tinnirello, M. 2010. Reduced toxicity, high performance monopropellant at the U.S. Air Force Research Laboratory. Presented at the 4th International Association for the Advancement of Space Safety Conference, Huntsville, AL, May 19–21.

Jankovsky, R.S., and Oleson, S.R. 1997. HAN-based monopropellant assessment for spacecraft. NASA Technical Memorandum 107287, AIAA-96-2863.

Juvan, K.C., and Beyer, R.A. 1999. A study of interaction of laser light with small drops of XM46 propellant and related liquids. ARL-TR-2053, U.S. Army Research Laboratory, Aberdeen Proving Ground, MD.

Katsumi, T., Inoue, T., Nakatsuka, J., Hasegawa, K., Kobayashi, K., Sawai, S., and Hori, K. 2012. HAN-based green propellant, application, and its combustion mechanism. *Combust. Explos. Shock Waves*, **48**, 536–543.

Khare, P. 2009. Decomposition and ignition of HAN-based monopropellants by electrolysis. M.S. thesis, Pennsylvania State University.

Kim, E.S., Lee, H.S., Mallery, C.F., and Thynell, S.T. 1997 Thermal decomposition studies of energetic materials using confined rapid thermolysis/FTIR spectroscopy. *Combust. Flame*, **110**, 239–255.

Kondrikov, B.N., Annikov, V.É., Egorshev, V.Y., and Luca, L.T. 2000 Burning of hydroxylammonium nitrate. *Combust. Explos. Shock Waves*, **36**, 135–145.

Kuwahara, T., Nakagawa, I., Hatano, H., Onda, T., and Takizuka, M. 1997. Thermal decomposition characteristics of HAN composite propellant. Presented at the 33rd Joint Propulsion Conference and Exhibit.

Lee, H., and Litzinger, T.A. 2001. Thermal decomposition of HAN-based liquid propellants. *Combust. Flame*, **127**, 2205–2222.

Lee, H., and Litzinger, T.A. 2003. Chemical kinetic study of HAN decomposition. *Combust. Flame*, **135**, 151–169.

Lee, Y.J., and Litzinger, T.A. 1999. Combustion chemistry of HAN, TEAN, and XM46. *Combust. Sci. Technol*., **141**, 19–36.

McQuaid, M., Burden, H., and Lawrence, W. 1998. Real-time laser-based detection of chemical intermediate formation in liquid propellant XM46 shock-loaded via an electric gun. ARL-TR-1625, U.S. Army Research Laboratory, Aberdeen Proving Ground, MD.

McQuaid, M., Watson, J., and Pilarski, D. 1998. UV/Vis emission from shock-loaded liquid propellant XM46. ARL-TR-1672, U.S. Army Research Laboratory, Aberdeen Proving Ground, MD.

Meng, H., Khare, P., Risha, G.A., Yetter, R.A., and Yang, V. 2009 Decomposition and ignition of HAN-based monopropellants by electrolysis. Presented at the 47th AIAA Aerospace Sciences Meeting, AIAA Paper 451.

Mueller, K.F., and Wagaman, K. L. 1999. Oxidizing agent. US Patent USH001768, January 5.

Risha, G.A., Yetter, R.A., and Yang, V. 2007. Electrolytic-induced decomposition and ignition of HAN-based liquid monopropellants. *Int. J. Energetic Mater. Chem. Propul*., **6**, 575–588.

Thakre, P., Duan, Y., and Yang, V. 2014 Modeling of ammonium dinitramide (ADN) monopropellant combustion with coupled condensed and gas phase kinetics. *Combust. Flame*, **161**, 347–362.

Van Dijk, C.A., and Priest, R.G. 1984 Thermal decomposition of hydroxylammonium nitrate at kilobar pressures. *Combust. Flame*, **57**, 15–24.

Vosen, S.R. 1989. Concentration and pressure effects on the decomposition rate of aqueous hydroxylammonium nitrate solutions. *Combust. Sci. Technol*., **68**, 85–99.

Wei, C., Rogers, W.J., and Mannan, M.S. 2006 Thermal decomposition hazard evaluation of hydroxylamine nitrate. *J. Hazard. Mater*., **130**, 163–168.

Yang, R., Thakre, P., and Yang, V. 2005. Thermal decomposition and combustion of ammonium dinitramide (Review). *Combust. Explos. Shock Waves*, **41**, 657–679.